

A BEM/RANS interactive method for predicting contra-rotating propeller performance

Yiran Su* and Spyros A. Kinnas^a

*Ocean Engineering Group, Department of Civil, Architectural and Environmental Engineering
The University of Texas at Austin, Austin, TX 78712, USA*

(Received September 15, 2017, Revised November 12, 2017, Accepted November 22, 2017)

Abstract. This paper introduces a BEM/RANS interactive scheme to predict the contra-rotating propeller (CRP) performance. In this scheme, the forward propeller and the aft propeller are handled by two separate BEM models while the interactions between them are achieved by coupling them with a RANS solver. By using the body force field and mass source field to represent the propeller in the RANS model, the number of RANS cells and the number of required RANS iterations reduce significantly. The method provides an efficient way to predict the effective wake, the steady/unsteady propeller forces, etc. The BEM/RANS interactive scheme is first applied to a CRP in both an axisymmetric manner and a non-axisymmetric manner. Results are shown in good agreement with the experimental data in moderate to high advance ratios. It is proved that the difference between the axisymmetric scheme and the non-axisymmetric scheme mainly comes from the non-axisymmetric bodies. It is also found that the error is larger at lower advance ratios. Possible explanations are given. Finally, some additional cases are tested which justifies that the non-axisymmetric BEM/RANS scheme is able to handle a podded CRP working at given inclination angles.

Keywords: contra-rotating propeller; boundary element method; CFD simulation; hydrodynamic analysis; propeller performance; BEM/RANS

1. Introduction

A contra-rotating propeller, also referred to as CRP, is a propulsion unit which includes two coaxial single propellers operating in opposite directions. The use of CRPs in marine propulsion significantly improves the fuel efficiency. It also helps underwater vehicles in maintaining torque balance.

To predict the CRP performance, the boundary element method (BEM), which has been proved to be successful and efficient for single-propellers, is limited. This is due to the fact that the aft propeller is subject to a vortical inflow, which is resulted by the forward propeller's trailing wake and the strut's trailing wake. Since the interactions between the vortical inflow and aft propeller's perturbation flow are beyond the extent of potential flow theories, using merely a BEM solver in predicting the CRP performance might lead to numerical error.

*Corresponding author, Ph.D. candidate, E-mail: yiransu@utexas.edu

^a Professor, E-mail: kinnas@mail.utexas.edu

A number of studies have been focused on the prediction of the CRP performance by either a potential method or a viscous method. Wang and Xiong (2013) performed hydrodynamic analysis of CRPs via RANS method and studied the effect from the time step size and the turbulence models. Paik *et al.* (2015) studied the wake evolution of a contra-rotating propeller by RANS. Liu (2009) used a panel method to predict the steady and unsteady CRP performance. In this application, the interactions between the vortical inflow and the propeller perturbation flow are neglected so that the forward propeller's perturbation flow field can be directly added to the background flow field of the aft propeller. Ghassemi and Taherinasab (2013) used a similar method for CRP design optimization. Davide *et al.* (2010) implemented a similar method and compared the numerical results with experimental data.

In order to incorporate the interactions between the vortical inflow and the propeller perturbation flow, the vortex lattice method (VLM) can be coupled with an axisymmetric RANS method (Stern *et al.* 1988, Gu and Kinnas 2003, Tian *et al.* 2014). In these applications, the total flow is solved by the RANS solver in which the propeller is represented by a body force field determined in the VLM solver. The RANS solution is then used to evaluate the effective wake. For CRP applications, two separate VLM models can be used, one for the forward propeller and the other for the aft propeller. Su and Kinnas (2017) extended the method to incorporate the blade thickness blockage effect into the RANS model by coupling the boundary element method (BEM) with an axisymmetric RANS method.

In this paper, the BEM/RANS interactive scheme is adopted and further extended. Instead of using the axisymmetric RANS solver, a three-dimensional RANS solver is used so that the circumferential variation of the body force field, mass source field, and effective wake field can be allowed. As a result, the scheme is able to handle non-axisymmetric bodies like strut, rudder, and ship hull. This can be very important for a podded CRPs because the strut may impose a strong influence upon the aft propeller. Such influence may generate unsteady forces and local cavitation.

This paper starts by describing the non-axisymmetric BEM/RANS interactive scheme and some considerations on how to handle the CRP application. Then the scheme will be applied to a contra-rotating propeller in both the axisymmetric manner (neglect the strut and free surface) and the non-axisymmetric manner (include the strut and free surface). Finally, the scheme is used to predict the CRP performance at different angles of inclination. Results are analyzed and compared to experimental measurements.

2. Methodology

The description of the numerical scheme consists of three major components: the BEM solver, the RANS solver, and the coupling scheme between the two. Some special considerations for CRP applications are also described in the last part of this section.

2.1 Boundary element method

The boundary element method has been widely used in the prediction of both wetted and cavitating propulsor performance at a wide range of advance ratios (Fine 1992). This is due to the fact that the boundary layer thickness on a marine propulsor is relatively small and the flow outside the boundary layer can be treated as inviscid.

The flow in the vicinity of a propeller, called the total flow U_T , can be decomposed to a

background flow U_{IN} and a propeller perturbation flow U_P , as shown in Eq. (1).

In Eq. (1), all the velocities are defined in the ship-fixed coordinate system. A similar equation can be written for the shaft-fixed coordinate system, as shown in Eq. (2). Here, $\vec{\omega}$ is the angular velocity of the propeller and \vec{R} is the radial coordinate vector in the cylindrical coordinate system. In propeller applications, BEM is usually applied in the shaft-fixed coordinate system because it eliminates the rotating motion of the propeller boundaries. The velocity fields can be easily transformed to the global coordinate.

$$\vec{U}_T = \vec{U}_{IN} + \vec{U}_P \tag{1}$$

$$\vec{U}_T^{(R)} = \vec{U}_{IN}^{(R)} + \vec{\omega} \times \vec{R} + \vec{U}_P^{(R)} \tag{2}$$

$$\vec{U}_T^{(R)} = \vec{U}_{IN}^{(R)} + \vec{\omega} \times \vec{R} + \vec{U}_P^{(R)} \tag{2}$$

In order to use the rotating coordinate system, BEM is usually used to solve the perturbation flow $\vec{U}_P^{(R)}$ while the background flow field is given and a set of boundary conditions are defined with respect to the total flow. Due to the thin boundary layer assumption, the perturbation flow is inviscid and governed by the Laplace equation. If the background flow is also inviscid and, thus, satisfies the Laplace equation, the total flow should also satisfy the Laplace equation because it is a linear equation.

The above conclusion is no longer true if the background flow is viscous (vortical). In this case, the background flow is governed by the nonlinear Navier Stokes equation and, therefore, the sum of the background flow and the perturbation flow does not provide a valid flow field. In other words, the propeller perturbation flow can impose an influence toward the background flow which leads to the so-called effective wake U_E .

$$\vec{U}_E = \vec{U}_T - \vec{U}_P \tag{3}$$

To solve the propeller perturbation flow with the boundary element method, the perturbation potential's Laplace equation can be inserted into the Green's third identity, as shown in Eq. (4). G is the Green's function for Laplace equation; S_B and S_w are propeller surfaces and blade trailing wake surfaces respectively; $\nabla\phi_w$ is the dipole strength on the trailing wake surfaces and can be determined by the Kutta condition; n is the normal vector on boundaries; ϕ is the perturbation potential which needs to be solved.

$$2\pi\phi = \iint_{S_B} \left[\phi \frac{\partial G}{\partial n} - G \frac{\partial \phi}{\partial n} \right] ds + \iint_{S_w} \left[\nabla\phi_w \frac{\partial G}{\partial n} \right] ds \tag{4}$$

By splitting the propeller surfaces and wake surfaces into panels and assigning constant strength sources and dipoles on every panel, Eq. (4) can be discretized to a set of linear equations. These equations can be solved efficiently by an iterative solver (Clark 1985).

2.2 RANS method

Although RANS can be used to predict the hydrodynamic performance of various types of marine propulsors, the computational efficiency may suffer when the unsteady performance is needed. More specifically, in a transient RANS simulation, the extremely small size of the cells near the propeller blades limits the time step size and hinders the overall computational efficiency.

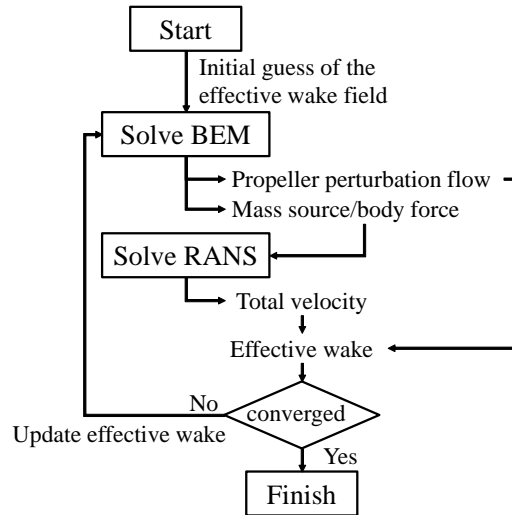


Fig. 1 Algorithm of the BEM/RANS interactive scheme

In this application, in order to improve the numerical efficiency, the RANS model does not explicitly treat the propeller blades by body-conforming mesh and non-slip wall-boundaries. Instead, a body force field F and a mass source field Q are used to represent the propeller blades. This significantly increases the size of the smallest cells in RANS and reduces the overall number of RANS cells.

Furthermore, by stating that the propeller is rotating fast enough so that the unsteady flow component can be decoupled, the unsteady RANS solver can be reduced to the steady RANS solver. It is worth mentioning that only the high-frequency unsteady component of the flow is dropped. The body force field, mass source field, and effective wake field are still allowed to vary in the circumferential direction.

Finally, the steady RANS equation with the added mass source field and body force field can be written as Eqs. (5) and (6).

$$\frac{\partial \bar{u}_j}{\partial x_j} = Q \quad (5)$$

$$\bar{U}_j \frac{\partial \bar{u}_i}{\partial x_j} = -\frac{1}{\rho} \frac{\partial P}{\partial x_i} + \nu \frac{\partial^2 \bar{u}_i}{\partial x_j \partial x_j} - \frac{\partial}{\partial x_j} \langle u_i u_j \rangle + F_i \quad (6)$$

2.3 BEM/RANS interactive method

As stated previously, when the background flow is viscous, the propeller perturbation flow imposes an influence toward the background flow and leads to the effective wake. In order to calculate this effective wake, the BEM solver needs to be coupled with the RANS solver.

The numerical algorithm of the BEM/RANS interactive scheme is shown in Fig. 1. In this algorithm, BEM is first solved with an initial guess of the effective wake field. The output of the BEM solver includes the body force field, the mass source field, and the propeller's perturbation flow field. Then, RANS can be solved with the body force field and the mass source field. The

output of RANS is the total flow field which can be used to calculate and update the effective wake via Eq. (2). It usually takes 4 to 9 iterations for the effective wake to converge; relaxation can also be added to boost the convergence or to improve the numerical stability.

In the previous research, in order to avoid the singularity in calculating the perturbation flow, the effective wake is often evaluated at an upstream location, either at a flat disk or at a curved surface that conforms to the shape of the blade leading edge. In these applications, the axial variation of the effective wake is not allowed. The effective wake at a BEM panel is assumed to equal to the effective wake velocity at a point on the upstream disk with the same radial and circumferential coordinates. According to Tian (2014), allowing the axial variation of the effective wake leads to better numerical accuracy. Therefore, the effective wake field is evaluated at the center of every blade panel in this paper.

In calculating the time-averaged perturbation flow field \vec{U}_p at a fixed point in the ship-fixed coordinate system, there might be a period when the point falls inside the thickness of a blade. There are at least two different approaches on how to treat this part of the perturbation flow in doing the time-averaging. The first method, according to the boundary element theory, treats the velocity inside the blade thickness as zero and performs the time-averaging in the whole blade-passing period. The second method, however, calculates the time-averaged perturbation flow in a shorter period, only when the point is located outside the blade thickness. It is evident that the first method leads to a perturbation flow that is weaker than that of the second method. In other words, the thickness blockage effect is not included in the time-averaged perturbation flow field of the first method. Therefore, in order to be consistent, the total flow should not include the mass sources in this situation. On the other hand, if the second method is used, the thickness blockage effect is included in the perturbation flow and, therefore, the mass source should also be included in RANS. In this paper, the second method is adopted. Detailed descriptions and parametric studies of the thickness blockage effect can be found in Su and Kinnas (2017).

The body force field \vec{F} is caused by the pressure jump between the two sides of a blade. The pressure jump $\Delta\vec{P}$ is first defined on the blade mean camber surface and calculated by summing the two pressure distributions on both sides of a blade. Then, a delta function is used to distribute the concentrated pressure jump into body force field, as shown in Eq. (7). In this equation, T is the blade-passing period, ω is the angular speed, θ is the circumferential coordinate, r is the radial coordinate of a panel, \mathbf{x} is a location vector, and the blade angle at time t is $\theta_B(t)$.

$$\begin{aligned} &= \frac{1}{T} \int_0^T \Delta\vec{P}[\theta_B(t)] \delta(|\mathbf{x}(\theta) - \mathbf{x}[\theta_B(t)]|) dt \\ \vec{F}(\theta) &= \frac{1}{\omega r T} \int_0^{2\pi} \Delta\vec{P}[\theta_B(t)] \delta(|\theta - \theta_B(t)|) d[\theta_B(t)] \\ &= \frac{\Delta\vec{P}(\theta)}{2\pi r} \end{aligned} \tag{7}$$

The mass source field Q represents the thickness blockage effect. The concentrated mass source ΔQ is first defined on the blade mean camber surface and calculated by adding the two BEM source distributions on both sides of the blade, as shown in Eq. (8). Then, the concentrated mass source is distributed into a mass source field using the same procedure as in Eq. (7).

$$\Delta Q = \sum_{\text{both sides}} - \left(\vec{U}_{IN}^{(R)} + \vec{\omega} \times \vec{R} \right) \cdot \vec{n} \quad (8)$$

When the mass source is included in the continuity equation, the local velocity may change. A positive mass source reduces the local velocity while a negative mass source increases the local velocity. This is due to the Lagally force and needs to be compensated by an extra body force field on top of the body force field calculated in Eq. (7). The compensating force field \vec{F}_C can be calculated by Eq. (9) where ρ is the flow density.

$$\vec{F}_C = -\rho \vec{U}_T Q \quad (9)$$

It is worth mentioning that the above non-axisymmetric scheme can be easily converted to its axisymmetric counterpart by doing the circumferential average of the body force field, mass source field, and perturbation flow field. Then, the axisymmetric RANS solver can be coupled with a steady BEM solver (Su and Kinnas 2017).

2.4 Special considerations for contra-rotating propellers

To implement the above scheme on CRPs, the RANS solver needs to be coupled with two separate BEM solvers: one for the forward propeller and the other for the aft propeller. By coupling BEM with RANS, the interactions between the two propellers are included.

Since the BEM solver is nondimensionalized by the propeller's maximum radius and the RANS solver is nondimensionalized by the forward propeller's maximum radius, the aft propeller's body force field and mass source field need to be scaled before they are used in RANS.

The size ratio m is defined by Eq. (10), where D_F and D_A are the maximum diameters for the forward propeller and the aft propeller respectively. According to the Buckingham- π theorem, the aft propeller's body force field F and mass source field Q can be scaled by Eqs. (11) and (12).

$$m = D_F/D_A \quad (10)$$

$$F_{\text{RANS}} = \frac{D_{\text{BEM}}}{D_{\text{RANS}}} F_{\text{BEM}} = m F_{\text{BEM}} \quad (11)$$

$$Q_{\text{RANS}} = \frac{R_{\text{BEM}}}{R_{\text{RANS}}} Q_{\text{BEM}} = m Q_{\text{BEM}} \quad (12)$$

3. Numerical models

In this paper, a podded CRP is used to validate the BEM/RANS interactive scheme. As shown in Fig. 2, the CRP includes a 3-blade forward propeller, a 4-blade aft propeller, a pod, and a strut. The BEM/RANS method is applied in three different cases: an axisymmetric case where the effect of the strut is neglected, a non-axisymmetric case where the strut is included in the RANS model, and a non-axisymmetric case at a given inclination angle.

3.1 Axisymmetric

In this application, a 2D-axisymmetric RANS model is coupled with two BEM models, as

shown in Fig. 3. The strut is neglected in both the RANS model and the BEM models. To ensure numerical stability, the downstream shaft geometry is modified in the aft BEM model. The $k-\omega$ SST turbulent viscosity model is used in the RANS solver. With a 2.7 GHz E5-2680 processor, it takes about 1 hour for the interactive scheme to converge. It is worth noting that both the forward propeller and the aft propeller are solved as right-handed propellers in BEM. The θ -body force and swirl effective wake are reversed in the interaction step between BEM and RANS.

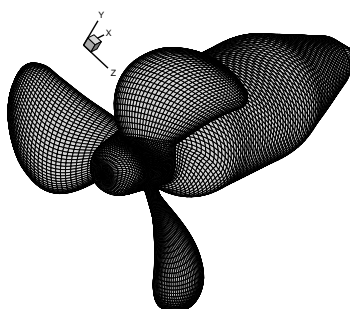
3.2 Non-axisymmetric with straight inflow

In this application, a three-dimensional RANS model, as shown in Fig. 4, is coupled with two BEM models, as shown in Fig. 3. Although the panel arrangement of both BEM models is the same between the non-axisymmetric case and the axisymmetric case, the BEM solver behaves differently in the two cases. The BEM solver in the axisymmetric application only solves for the mean propeller performance while the BEM solver in the non-axisymmetric case solves for the propeller performance as a function of the blade angle.

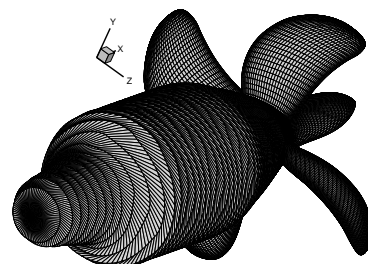
In the RANS model, the strut is represented by non-slip walls while the free surface and the pod are simplified to slip walls. With four 2.7 GHz E5-2680 processor, it takes around 5 hours for the interactive scheme to converge.



Fig. 2 Geometry of the contra-rotating propeller



(a) Forward BEM model



(b) Aft BEM model

Fig. 3 BEM models for the contra-rotating propeller (for both the axisymmetric case and the non-axisymmetric case)

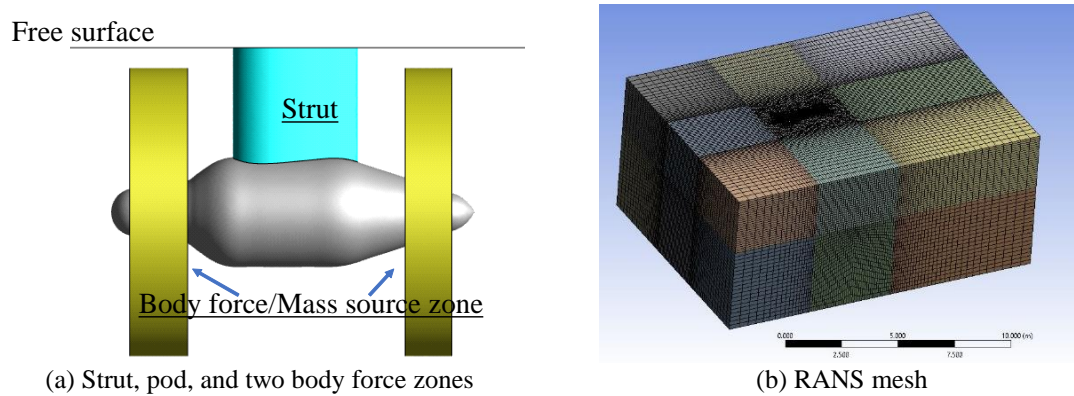


Fig. 4 Three-dimensional RANS model geometry

3.3 Non-axisymmetric with inclined shaft

This application considers the same CRP geometry working in a horizontally-inclined situation. The center axis of the shaft is rotated toward either the port side or the starboard side. We define the inclination towards the starboard side to be positive and test several different angles of inclination ranging from -10 degrees to +10 degrees.

Instead of rotating the CRP geometry, it is easier to solve the problem in a rotated coordinate system. Therefore, the same BEM models are used as those in the straight-inflow case. The RANS model is also the same as the straight-inflow case except the inflow direction is changed by the inclination angle.

4 Results and comparison

In this section, the dimensionless numbers are defined by using the forward propeller diameter D_F , ship speed V_S , and the propeller rotation speed n (RPS) as variables. The definition of advance ratio J_S , thrust coefficient K_T , torque coefficient K_Q , and the dimensionless blade circulation G_S are given in Eq. (13), where T is the thrust, Q is the torque, and Γ is the blade circulation.

$$J_S = \frac{V_S}{nD_F} \quad K_T = \frac{T}{\rho n^2 D_F^4} \quad K_Q = \frac{Q}{\rho n^2 D_F^5} \quad G_S = \frac{100\Gamma}{\pi D_F V_S} \quad (13)$$

4.1 Convergence study

A convergence study is first made to test whether the propeller performance is sensitive to the number of panels in the BEM model and the number of the cells in the RANS model. As shown in Table 1, the non-axisymmetric version of the BEM/RANS interactive scheme is tested in two cases. Compared to case A, case B has a higher number of panels in both BEM models and a higher number of RANS cells near the propeller region. The circulation distributions on the forward propeller and aft propeller are compared, as shown in Fig. 5. The total thrust coefficients

predicted by case A and case B are 0.388 and 0.386 respectively, with a 0.37% difference between the two.

4.2 Comparisons between axisymmetric cases and non-axisymmetric cases

If we only care about the CRP’s mean performance, the non-axisymmetric component of the flow can be neglected and the axisymmetric version of the BEM/RANS scheme can be used. However, it is very important to know how much numerical error can be made by neglecting the non-axisymmetric flow component.

Before making further statements, it is helpful to think about what assumptions are made in reducing the non-axisymmetric problem to the axisymmetric problem. First, the non-axisymmetric bodies, meaning the strut and the free surface in this case, are neglected. Then, the three-dimensional RANS equations are integrated along the circumferential direction. If we assume the total flow does not change much in the circumferential direction, the crossing terms, which are created in the integration of the convective terms, can be neglected. Then, the 3D RANS equation can be written into its axisymmetric form (Su and Kinnas 2017).

In Fig. 6, the single-blade thrust coefficient and torque coefficient are shown as a function of the blade position angle. 0-degree corresponds to the blade location when it passes strut.

Table 1 Number of panels/cells used in the convergence study

	Forward BEM Model	Aft BEM Model	RANS Model
Case A	1200	1200	1.6 million
Case B	2400	2400	2.2 million

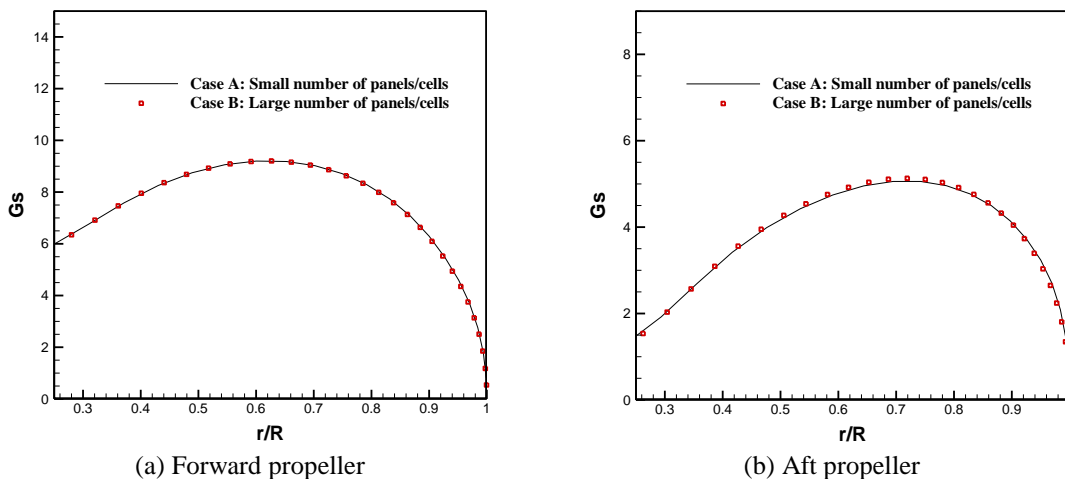


Fig. 5 Comparison of the mean blade circulation between case A (small number of panels/cells) and case B (large number of panels/cells)

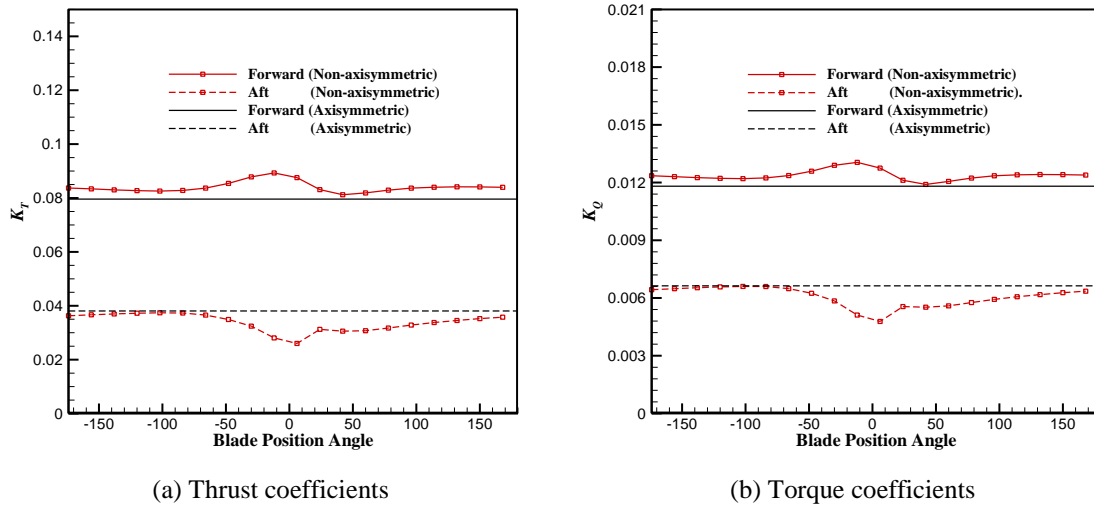


Fig. 6 Comparisons on the unsteady thrust coefficients and torque coefficients

In the non-axisymmetric case, at around the 0-blade-angle, where the blades are closest to the strut, both K_T and K_Q from the forward blade increase while both K_T and K_Q from the aft blade decrease. In the axisymmetric case, K_T and K_Q do not change with the blade position angle. More importantly, both K_T and K_Q in the axisymmetric case are very close to the K_T and K_Q in the non-axisymmetric case except when they are close to the 0-blade-angle. Therefore, it is fair to say that the difference between the axisymmetric BEM/RANS and the non-axisymmetric version mainly comes from the non-axisymmetric bodies. Neglecting of the crossing terms does not make much difference and can be seen as a reasonable assumption.

In Fig. 7, the thrust coefficients and torque coefficients are compared with experimental data at different advance ratios (Jukola). These coefficients are given by individual propeller values as well as the total CRP values. The total thrust includes not only thrust on both propellers but also the negative drag forces on the pod and on the strut. As the figure shows, results from both the axisymmetric scheme and the non-axisymmetric scheme have a good agreement with the experimental data. Similar to what has been discovered before, neglecting the strut and the free surface leads to a lower forward propeller loading and a higher aft propeller loading.

At lower advance ratios, the error becomes noticeable. A possible explanation can be made by looking at the assumptions of the BEM/RANS interactive scheme. If we start from the more general unsteady RANS equation and integrate them with respect to time over a blade-passing period, the steady RANS equation can be obtained with several additional crossing terms originated from the convective term. If a small amplitude assumption is made on the unsteady component of the total flow, the crossing term can be neglected. It is important to mention that the propeller perturbation flow field, which rotates with the propeller, is the major source of the unsteady flow component. At normal advance ratios, the small amplitude assumption is reasonable. However, as the advance ratio becomes extremely low and the propeller loading gets enough high, the stronger propeller perturbation flow leads to a more significant unsteady component. In this case, the small amplitude assumption may no longer be valid and, therefore, the error may increase.

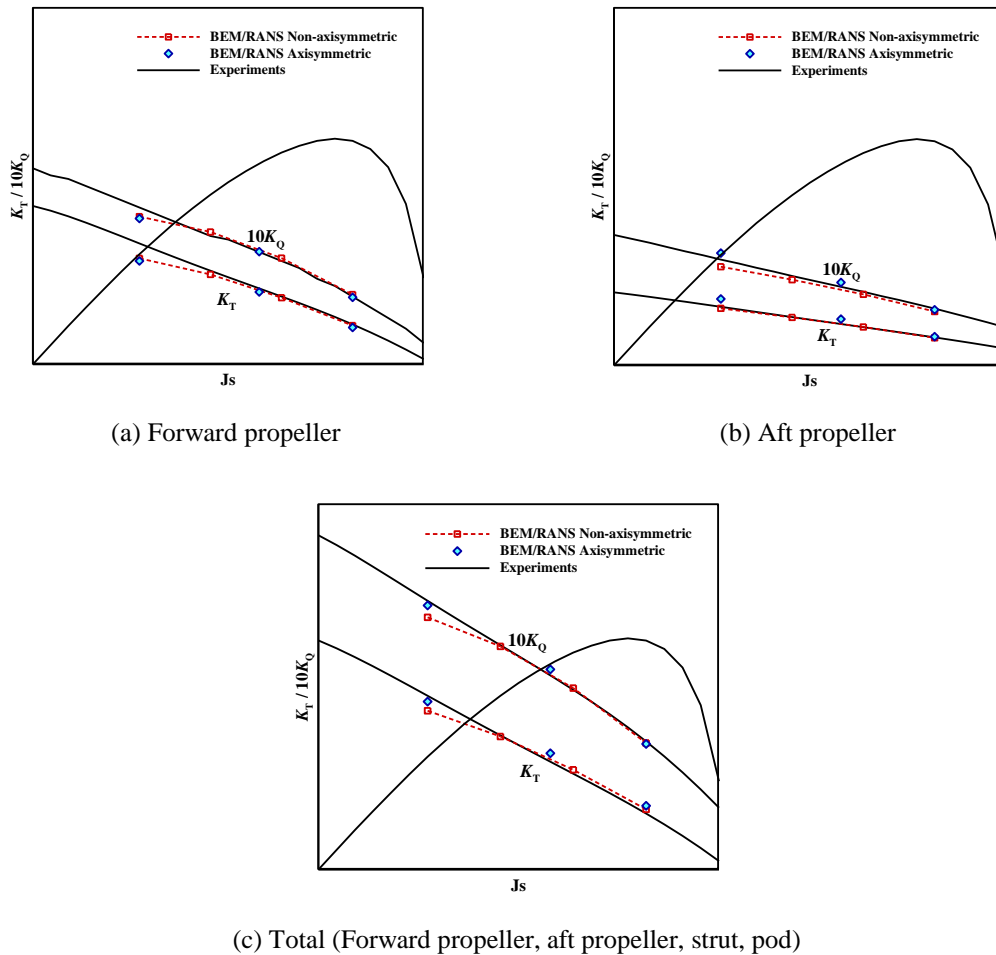


Fig. 7 Comparison of the predicted thrust coefficients and torque coefficients with experimental data (all 3 figures are plotted with the same scale)

For the total forces in low advance ratios, as shown in Fig. 7(c), the axisymmetric scheme has a relatively smaller error compared to the non-axisymmetric scheme. This cannot be interpreted as axisymmetric behaves better because the lower error comes from the cancellation between an underpredicted forward propeller force and an overpredicted aft propeller force. The overpredicted aft propeller loading, as we discussed before, is due to the lack of the strut effect.

In Fig. 8, the axial body force, circumferential body force, and mass source in the non-axisymmetric case are plotted near the propeller region. The forward propeller and the aft propeller both generate a positive axial body force while the circumferential body forces they induced are in opposite directions. The mass source reflects the gradient of the blade thickness distribution in the flow direction. Therefore, it should be positive near the leading edge and negative near the trailing edge. Also, the volume integration of the mass source field should be close to zero.

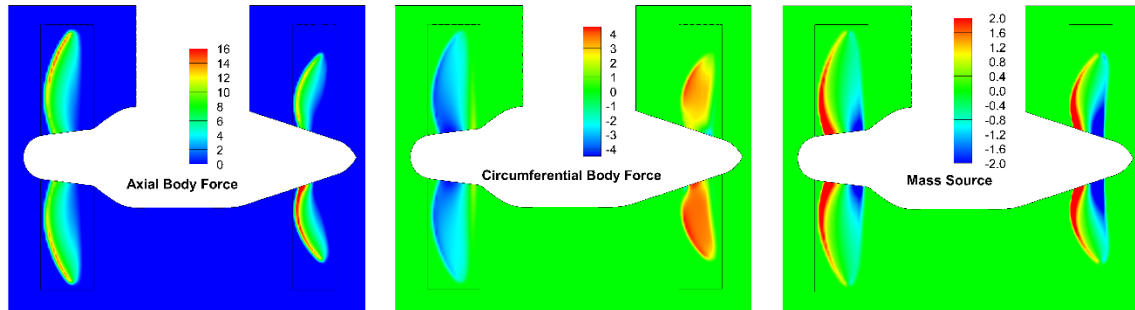


Fig. 8 Body force distribution and mass source distribution from the non-axisymmetric BEM/RANS case; the body force field is nondimensionalized by $(2\rho V_S^2/D_F)$ and the mass source field is nondimensionalized by $(2\rho V_S/D_F)$. The forward propeller is on the left side of every plot

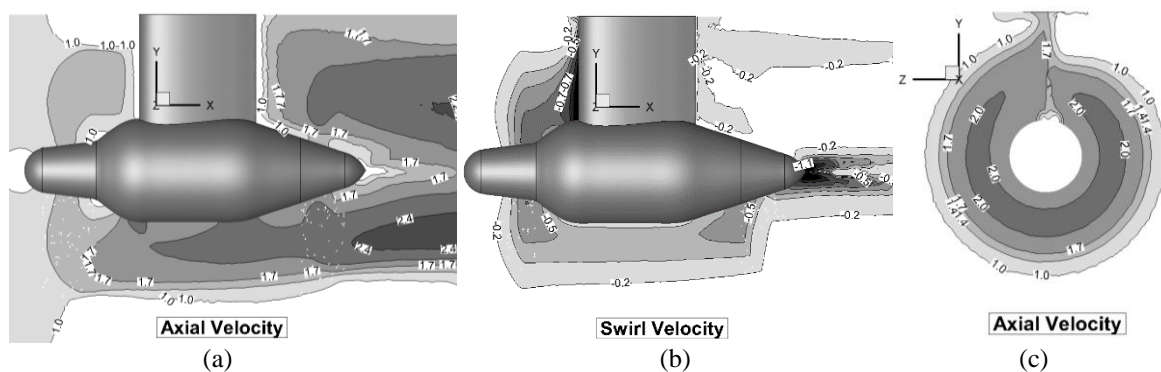


Fig. 9 (a) axial and (b) swirl component of the total flow plotted on the ship center plane and (c) axial component of the total flow plotted on a station between the strut's trailing edge and the aft propeller's leading edge. The velocity is nondimensionalized by the ship speed V_S .

Fig. 9 shows the axial and swirl components of the total flow on the ship center plane as well as the axial component of the total flow at a station between the strut's trailing edge and the aft propeller's leading edge. In Fig. 9(b), the swirl component of the flow induced by the forward propeller is canceled by the aft propeller while a small leakage happens near the hub. In Fig. 9(c), the boundary layer of the strut can be clearly seen.

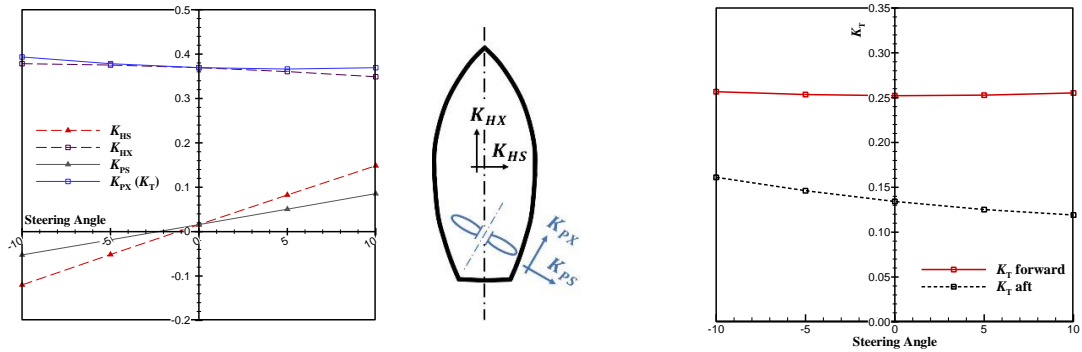
4.3 Non-axisymmetric case with inclined shaft

In a podded CRP application, it is useful to predict the forces generated by the CRP unit when it is working at an angle of inclination. To simplify this, the unsteady maneuvering problem, which involves a nonuniform and unsteady background flow, is reduced to a steady uniform-inflow inclined-shaft problem.

The non-axisymmetric version of the BEM/RANS scheme is used. The predicted forces generated by the CRP at different inclination angles are shown in Fig. 10. Fig. 10(a) includes 4

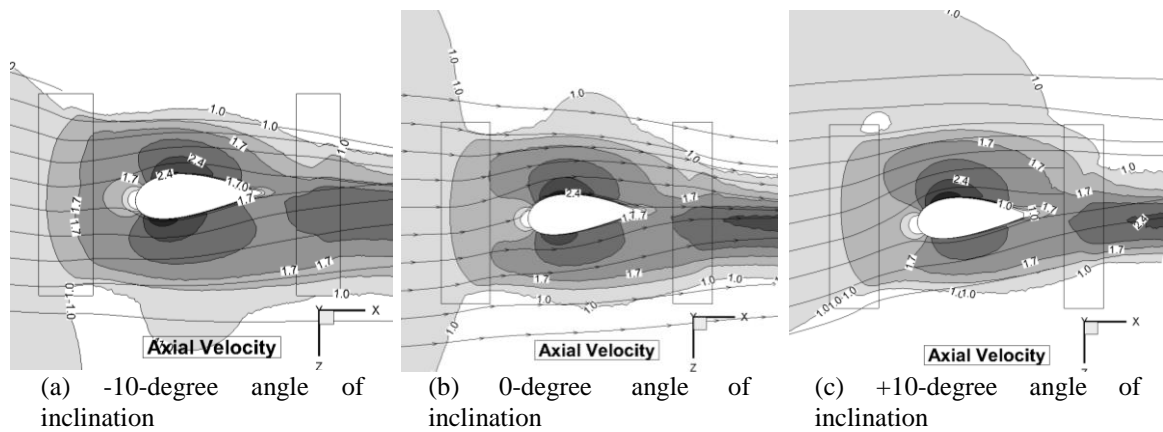
different components of the total force, all of which are non-dimensionalized by $\rho n^2 D_F^4$. Force K_{HX} and K_{HS} are forces in the longitudinal direction and the horizontal direction of the ship hull coordinate system. Force K_{PX} and K_{PS} are forces in the axial direction and the horizontal direction of the propeller axis coordinate system. Both of the horizontal forces define their positive direction as pointing from the port side to the starboard side. K_{PX} is equivalent to the propeller's thrust coefficient. Fig. 10(b) shows the contribution of the total thrust coefficients from either the forward propeller or the aft propeller.

Fig. 11 shows the axial component of the total flow on a horizontal plane at the mid-span of the strut. In Fig. 12, the effective wake of the aft propeller is plotted on the mid-chord propeller disk. The axial velocity is represented by the grayscale while the other components of the velocity are shown by arrows. The effective wake field can vary, though, in the axial direction.



(a) Projections of total force in four different directions (b) Thrust coefficient from both propellers

Fig. 10 Propeller forces at different angles of inclination



(a) -10-degree angle of inclination (b) 0-degree angle of inclination (c) +10-degree angle of inclination

Fig. 11 Axial total flow distribution on the waterline plane near the half-span of the strut. The velocity is nondimensionalized by the ship speed V_S

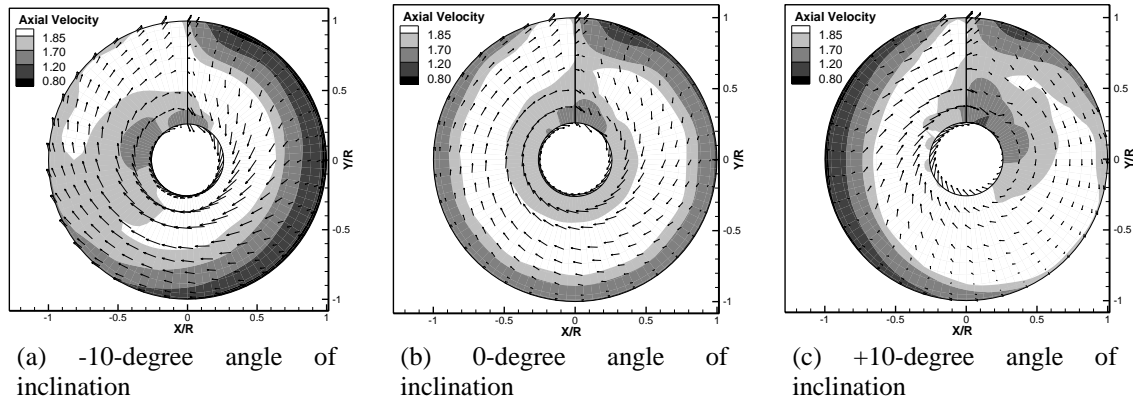


Fig. 12 Effective wake field of the aft propeller at different angles of inclination. The wake field is plotted on the mid-cord disk of the aft propeller. The velocity is nondimensionalized by the ship speed V_S

As shown in Fig. 10(a), when the inclination angle increases, force K_{HX} remains nearly unchanged while force K_{HS} grows linearly with the angle of inclination. In the propeller axis coordinate system, the horizontal force is linear to the angle of inclination while the axial force remains nearly constant. From Fig. 10(b), the thrust of the forward propeller does not change much within 10 degrees of inclination while the thrust of the aft propeller has a negative correlation with the angle of inclination. This can be explained by the effect of the strut. As the angle of inclination increases, the strut-induced downstream swirl velocity increases. This leads to an increased aft propeller loading and, thus, an increased thrust coefficient.

From Fig. 12, the effective wake field for the aft propeller has a strong axial component and a strong swirl component. At the ± 10 angle of inclination, part of the aft propeller falls outside of the forward propeller's trailing wake region. At the outside region, both the axial component and the swirl component of the effective wake become weaker.

Based on the above results, the non-axisymmetric BEM/RANS interactive scheme is capable of handling a CRP propeller working at an inclination angle. Correlations with experiments are needed in the future when experimental data becomes available.

5 Conclusions

In this paper, a BEM/RANS interactive scheme is applied to a contra-rotating propeller (CRP). In this scheme, the propeller performance is solved by the BEM model while the interactions between the forward propeller and the aft propeller are handled in a time-averaged sense via coupling the BEM solvers with the RANS solver. The method was applied to a CRP unit in both the axisymmetric manner and the non-axisymmetric manner. Results show good agreement with the open water test results. Finally, the method is applied to the same CRP geometry at different angles of inclination.

Both the axisymmetric scheme and the non-axisymmetric scheme behave well in terms of predicting the mean performance. However, the non-axisymmetric scheme is able to consider the

effect of the strut and the effect of the free surface. As a result of the strut and the free surface, the forward propeller's loading increases as any one of its blades moves close to the strut. The aft propeller's loading decreases as any one of its blades move close to the strut. The non-axisymmetric scheme is also able to handle the non-uniform inflow situations and the inclined shaft situations more accurately.

Future work includes considering the ship motion as well as the ship hull's trailing wake in evaluating the effective wake. This leads to a more realistic situation. A complete BEM/RANS scheme can also be implemented by coupling the BEM solver with an unsteady RANS solver. This unsteady scheme does not rely on the assumption that the propeller perturbation velocity is relatively smaller than the background flow. Therefore, it may behave better than the time-averaged approach in extreme low advance ratios. The BEM/unsteady-RANS interactive scheme also enables the simulation of unsteady ship maneuvering.

Acknowledgements

Support for this research was provided by the U.S. Office of Naval Research (Grant No. N00014-14-1-0303; Dr. Ki-Han Kim) and Phase VII of the "Consortium on Cavitation Performance of High Speed Propulsors" with the following members: Kawasaki Heavy Industry Ltd., Rolls-Royce Marine AB, Rolls-Royce Marine AS, SSPA Sweden AB, Andritz Hydro GmbH, Wärtsilä Netherlands B.V., Wärtsilä Norway AS, Wärtsilä CME Zhenjiang Propeller Co. Ltd., and Steerprop Ltd.

References

- Clark, R.W. (1985), "A new iterative matrix solution procedure for three-dimensional panel methods", *AIAA 23rd Aerospace Sciences Meeting*, Nevada, USA, January.
- Fine, N.E. (1992), "Nonlinear analysis of cavitating propellers in nonuniform flow", Ph.D. dissertation, Massachusetts Institute of Technology, Boston.
- Ghassemi, H. and Taherinasab, M. (2013), "Numerical calculations of the hydrodynamic performance of the contra-rotating propeller (CRP) for high-speed vehicle", *Polish Maritime Res.*, **20**(2), 13-20.
- Grassi, D., Brizzolara, S., Viviani, V., Savio, L. and Caviglia, S. (2010), "Design and analysis of counter-rotating propellers-comparison of numerical and experimental results", *J. Hydrodynamics, Ser. B*, **22**(5), 570-576.
- Gu, H. and Kinnas, S.A. (2003), "Modeling of contra-rotating and ducted propellers via coupling of a vortex-lattice with a finite volume method", *Proceedings of the Propeller/Shafting 2003 Symposium*, Virginia Beach, USA, September.
- Jukola, H., Steerprop Ltd. (Private communication)
- Liu, X.L. (2009), "A potential based panel method for prediction of steady and unsteady performances of contra-rotating propellers", *Proceedings of the 1st International Symposium on Marine Propulsors*, Trondheim, Norway, June.
- Paik, K., Hwang, S., Jung, J., Lee, T., Lee, Y., Ahn, H. and Van, S. (2015), "Investigation on the wake evolution of contra-rotating propeller using RANS computation and SPIV measurement", *Int. J. Naval Architect. Ocean Eng.*, **7**(3), 595-609.
- Stern, F., Kim, H., Patel, V. and Chen, H.A. (1988), "Viscous-flow approach to the computation of propeller-hull interaction", *J. Ship Res.*, **32**(4), 246-262.
- Su, Y. and Kinnas, S.A. (2017), "A generalized potential/RANS interactive method for the prediction of

- propulsor performance”, *J. Ship Res. Append.*, **61**(4), 214-229.
- Tian, Y., Jeon, C.H. and Kinnas, S.A. (2014), “Effective wake calculation/application to ducted propellers”, *J. Ship Res.*, **58**(2), 1-13.
- Wang, Z. and Xiong, Y. (2013), “Effect of time step size and turbulence model on the open water hydrodynamic performance prediction of contra-rotating propellers”, *China Ocean Eng.*, **27**(2), 193-204.

QM